Materials Science & Engineering A 614 (2014) 250–263

Contents lists available at ScienceDirect

Materials Science & Engineering A

journal homepage: www.elsevier.com/locate/msea

Evolution of deformation and annealing textures in Incoloy 800H/HT via different rolling paths and strains

Hamed Akhiani*, Majid Nezakat, Jerzy A. Szpunar

Department of Mechanical Engineering, University of Saskatchewan, Saskatoon, Canada

ARTICLE INFO

Article history:
Received 28 May 2014
Received in revised form
8 July 2014
Accepted 11 July 2014
Available online 19 July 2014

Keywords:
Incoloy 800H/HT
Annealing texture
Deformation texture
Cross-rolling

ABSTRACT

In this report, we characterize the deformation and annealing textures of Incoloy 800H/HT, following different rolling conditions that produced different textures in this material. Incoloy 800H/HT is an austenitic Fe–Ni super alloy and is considered to be a candidate material for Gen IV nuclear reactors. Fossil fuel plants have used this alloy for decades; however, as grain structure and texture parameters can strongly affect its physical and mechanical properties in-service, engineers should consider some structural modifications before using this alloy in nuclear reactors.

In this study, we used Thermo-Mechanical Processing (TMP) to alter the texture of Incoloy 800H/HT. We applied various thickness reductions (10%, 30%, 50%, 70%, and 90%) to this alloy using two different rolling paths, followed by annealing. Our detailed study of the deformation and annealing texture evolution shows that upon different rolling paths, the final deformation texture and the annealing texture were different. Brass texture was the dominant component for the uni-directional rolled (UDR) samples, while a combination of brass (B) and ND-rotated brass (B_T) were the dominant components in the cross-rolled (CR) samples. Annealing textures of UDR samples were mainly Goss, copper, S, recrystallized brass ($\{236\}\langle 385\rangle$) and minor copper twin $\{552\}\langle 115\rangle$ components. At lower deformations ($< 50\%$), the annealed CR samples showed tilted cube, S, recrystallized brass ($\{236\}\langle 385\rangle$) and minor Goss twin $(113)\langle\overline{3}32\rangle$. However, at higher rolling reductions, the $B+B_T$ deformation texture was retained for the CR samples.

1. Introduction

Gen IV nuclear reactors use new concepts and designs to increase efficiency and improve safety. A Very High Temperature Reactor (VHTR) and a Super-Critical Water Reactor (SCWR) are among the designs selected for Gen IV reactors in the United States and Canada [1,2]. Both types are expected to work at high service temperatures (VHTR: 750–950 °C, SCWR: 550–650 °C) for a high thermodynamic efficiency [3]. Operating at high temperature/pressure requires materials with superior high temperature oxidation resistance. According to the Gen IV roadmap [1], Incoloy 800H/HT is one of the candidate materials for use as both cladding and structural components for the SCWR. It is notable that, in the very recent roadmap update (2014) [2], the candidate materials have been limited to austenitic steels with more than 20% chromium. Table 1 shows the chemical composition of Incoloy 800H/HT. Evidently this alloy with high chromium content still remains in this category.

Incoloy 800H/HT can be used for construction of various high temperature components in Gen IV reactors, including steam generators, intermediate heat exchangers, hot ducts, and fuel claddings [3–5]. Incoloy 800H/HT is a variant of the well-known austenitic Incoloy 800 family, which has chemical composition and heat treatment restrictions [6,7]. This alloy has been used widely in chemical processing, industrial heating and power generation units. Thus, there is a fairly good database on its behavior at high temperature. However, because of differences in the service conditions, some properties (e.g. grain boundary diffusion and corrosion resistance) should be improved. Several studies reveal that many important properties depend on grain boundary structure and texture [5,8–10].

Moreover, it is well known that the texture of FCC alloys has significant influence on mechanical properties, as well as oxidation resistance. Because the presence of strong texture can influence a wide range of mechanical properties, significant attention is paid to the control of two critical processing parameters, strain path and deformation temperature, which are key in deciding the final deformation texture. While deformation temperature has been widely studied for a variety of alloys, the strain path effect studies are limited to a few publications [11–13]. These studies show that the strain path can govern the deformation

* Corresponding author.
E-mail addresses: akhiani@gmail.com, hamed.akhiani@usask.ca (H. Akhiani).

http://dx.doi.org/10.1016/j.msea.2014.07.035
0921-5093/

Table 1
Chemical composition (wt%) of Incoloy 800H/HT.

Fe	Ni	Cr	Mn	Al	Ti	Mo	Cu	Si	Co	P	C	S
45.41	30.19	20.5	0.98	0.55	0.54	0.42	0.4	0.32	0.3	0.22	0.07	0.0001

texture and, accordingly, it might affect the recrystallization texture. The strain path can be changed by altering the rolling direction by some degrees about normal direction (ND) (e.g. 90° in cross-rolling) between the reduction passes. Cross-rolling will result in a different texture with lower anisotropy, intergranular misorientation, and fraction of low angle grain boundaries compared to unidirectional rolling in pure Ni and Cu [11,12]. In spite of these textural modifications, no serious attempts have been made at applying cross-rolling in Incoloy 800H/HT.

Furthermore, Stacking Fault Energy (SFE) as an alloy characteristic factor can influence the deformation and annealing textures of FCC materials. In high SFE materials, dislocation slip is a dominant deformation mechanism, thus no twinning occurs. The typical deformation textures of the FCC materials consist of copper (Cu), S and brass (B) components. On the contrary, in low SFE alloys (e.g. 800H/HT), the B texture would be the dominant texture with weak Cu and S components [12,14,15]. Twinning also has a significant effect on texture in low SFE FCC materials [16–19]. The smaller the SFE, the higher the contribution from deformation twins [20]. In addition, large grains have a higher tendency to deform by twinning, compared with small grains [21,22]. As twinning occurs in the deformation and annealing stages, it might influence both the deformation and annealing textures. The effect of twinning on texture was first described by Wassermann [19]. In his model, the volume of the deformation twins is related to texture transformation. Based on this model, the Cu component transforms to the Cu twin component {552}⟨115⟩ via twinning, which can be further transformed to a G component {110}⟨001⟩ by slip [19,23,24]. However, Leffers [21,23], and Sekine and Wang [20] experimentally show that this theory does not agree with the microstructural studies. They claim that the volume fraction of twins is not high enough to have a direct effect on the texture. Consequently, a second theory was introduced regarding the indirect effect of twinning on texture. In a highly twinned sample, the fine twin lamellae make slip difficult, hence imposing a microstructural hardening. By increasing the deformation strain, a glide mechanism would be activated to accommodate the strain increase. In such a way, twinning could indirectly affect the texture. Therefore this theory is called the overshooting/latent hardening twinning effect [20–23].

Nevertheless, the twinning volume effect still can be responsible for the texture development in very highly twinned materials. In other materials, microstructural latent hardening or the overshooting effects of twin lamellae play a significant role in texture transformation [20,21]. Sekine and Wang [20] show that in Ag with low SFE, a large number of Cu {112}⟨111⟩ grains decay to the Cu component {552}⟨115⟩ by normal Wassermann's twinning mode. By subsequent slip deformation, it can be transformed to {110}⟨112⟩ through G {110}⟨001⟩ orientation, resulting in a brass deformation texture. In addition, by comparing texture transition between very low SFE (Ag–Zn alloys) and low SFE (Ag) materials, these authors claim that the presence of {111}⟨110⟩ component shows that it is a characteristic deformation texture component that can be formed solely in very low SFE materials and results from overshooting/latent hardening in these materials [20].

Although there are rather controversial debates on the origin of deformation texture in low SFE FCC materials, the final textures are almost identical [16,21,24]. However, the recrystallization (annealing) textures of these materials show more discrepancy.

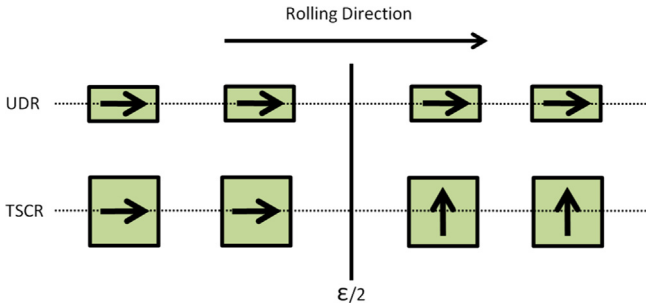

Fig. 1. Schematic graph showing the UDR and CR modes.

Nucleation and growth competition play a significant role in the formation of the annealing texture. “Oriented nucleation” and “oriented growth” are the two distinct models used to describe the texture evolution upon annealing [16,22]. The dominant mechanism depends on many factors such as the materials deformation state (driving force for recrystallization), grain boundary structure (misorientation: high and low angle boundaries), dislocation density, twinning, size of the nuclei, etc. Based on these factors both of these mechanisms can act competitively and simultaneously [16,18,22].

High SFE materials (e.g. Al, Cu) that show copper deformation texture form a dominant cube recrystallization texture. This has been related either to selective/oriented growth or oriented nucleation mechanisms [16,22,25]. For low SFE materials exhibiting brass deformation texture, various recrystallization components regarding the SFE have been reported. However, one of the most common recrystallization texture components is {236}⟨385⟩ known as recrystallization brass (R-brass) [26–30]. As Lucke states [31], this component in annealing texture intensifies as the SFE decreases. Sztwiertnia [26] claims that this orientation forms mainly upon oriented growth and favors materials with brass deformation textures.

Most of the aforementioned textural studies were performed on model copper, brass and silver alloys. To our knowledge, there is no comprehensive study on the texture evolution of Incoloy 800H/HT. A few studies focus on the Grain Boundary Engineering (GBE) of this alloy; however only very low deformations with normal unidirectional rolling were studied [6,10]. In recent years, following the devolvement of TWIP steels in the automotive industry, some studies have been done on these steels [24,28]. Although the texture evolution of TWIP and iron-based superalloys (i.e. Incoloy 800H/HT) share some common features, the strain-induced martensite in TWIP steels would alter the deformation and annealing textures [28].

In this paper we report the texture evolution of Incoloy 800H/HT via unidirectional and cross-rolling in both deformation and annealing states. Understanding the deformation and recrystallization behavior of this alloy under low and heavy deformation through different strain paths would be of significant value in optimizing its properties to suit prospective new applications (e.g. as a nuclear structural material).

2. Experimental procedure

For this study we used commercial Incoloy 800H/HT, which is a variant of Incoloy 800 [7]. Table 1 lists its chemical composition.

The alloy was fully annealed at 1420 °C and water quenched in as-received condition. We performed Thermo-Mechanical Processing (TMP) on the as-received sample by a series of cold rolling operations followed by annealing at 1050 °C for a time period of 25 min/cm thickness of the samples. We applied a true strain of 0.2 per rolling pass for all the samples, which were rolled to 10%, 30%, 50%, 70% and 90% thickness reductions with two different strain paths. We designed the experiments to allow us to decipher the roles of reduction percentage and strain path on the deformation and annealing textures. From the same plate we cut samples of $50 \times 50 \times 13.25\ mm^3$ and $50 \times 25 \times 13.25\ mm^3$ and subjected them to two modes of rolling with a laboratory roll machine to produce the thickness reductions. Fig. 1 illustrates the schematic of unidirectional rolling (UDR) and two-step cross-rolling (TSCR/CR) modes.

Textural studies employed a Bruker D8 X-ray diffractometer with Eulerian cradle using Cr-Kα, and a Vantec-500 detector with a 0.8 mm collimator. We used incomplete pole figures to calculate Orientation Distribution Function (ODF) as well as the texture component, by means of ResMat® software. The volume fractions of various texture components were calculated within 15° tolerance around their ideal position in the Euler space, both in micro and macrotexture. We made the microtexture measurements using an Oxford Electron Back Scatter Diffraction (EBSD) setup fitted on a Hitachi SU6600 Field Emission Gun Scanning Electron Microscope. The SEM was operated at 30 kV with the automatic EBSD scan. We performed EBSD on the TD plane as the planar features of cold-rolled microstructures can be better detected in this plane than on any other specimen plane. We used the HKL Technology Channel-5 software to carry out data analysis.

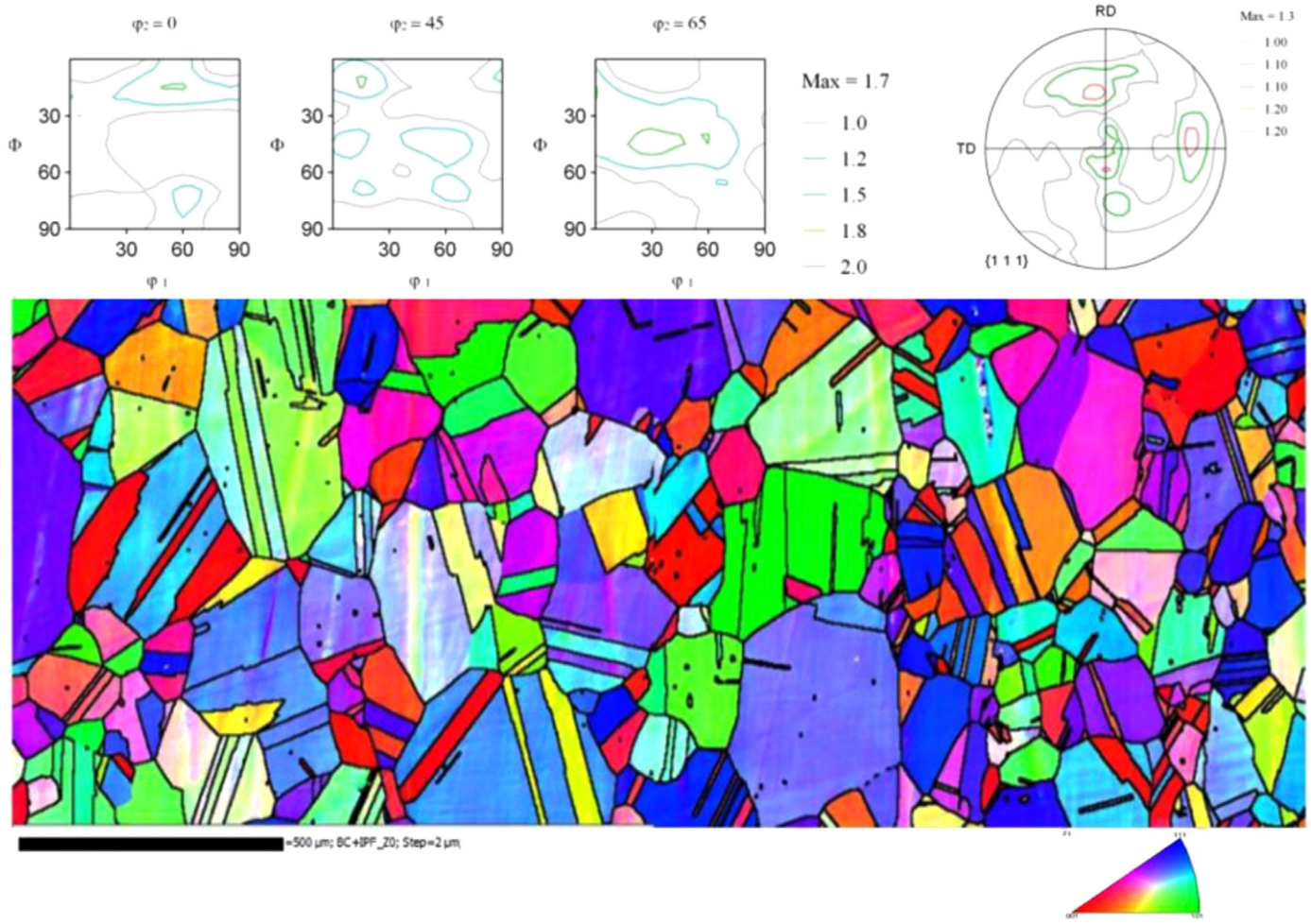

Fig. 2. ODF sections and Inverse Pole Figure (IPF) EBSD map of the starting Incoloy 800H/HT showing grain morphology and orientations.

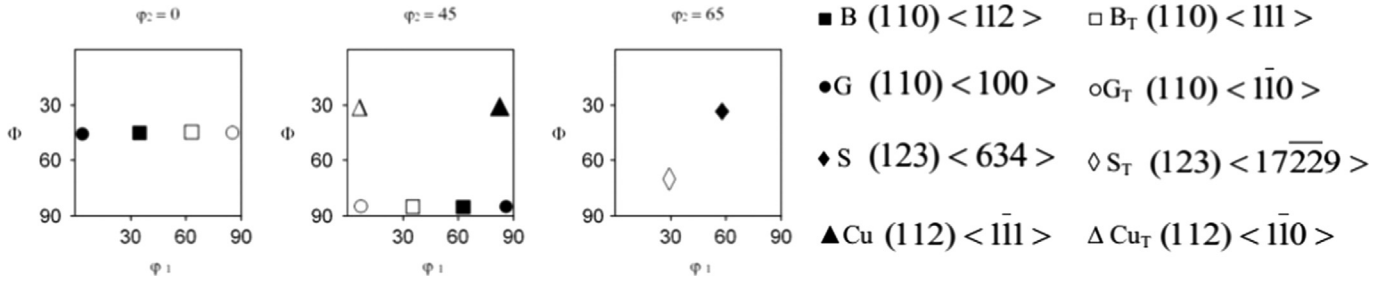

Fig. 3. Incoloy 800H/HT major texture components and their positions in the ODF sections.

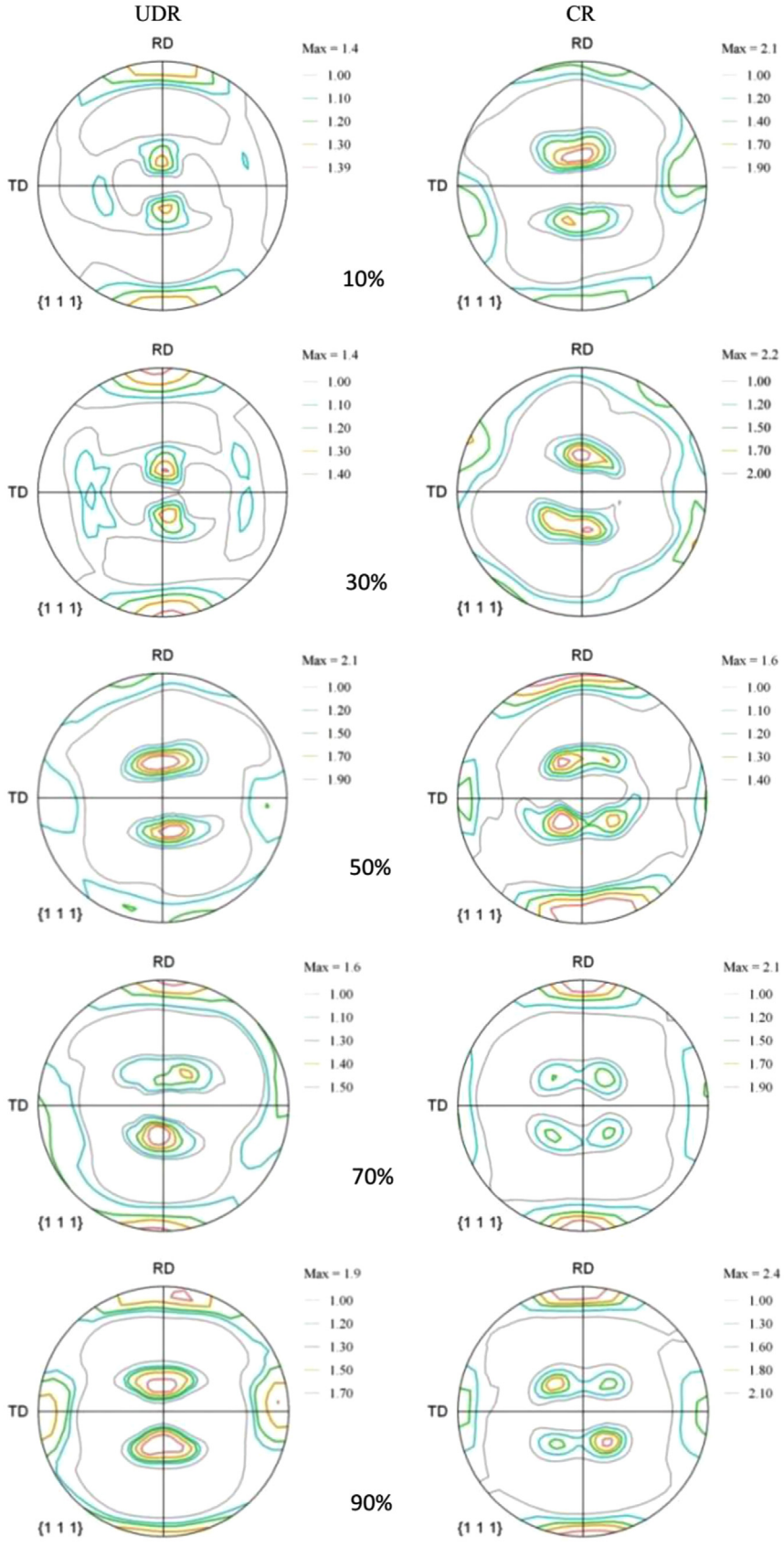

Fig. 4. (111) PFs of the CR and UDR samples.

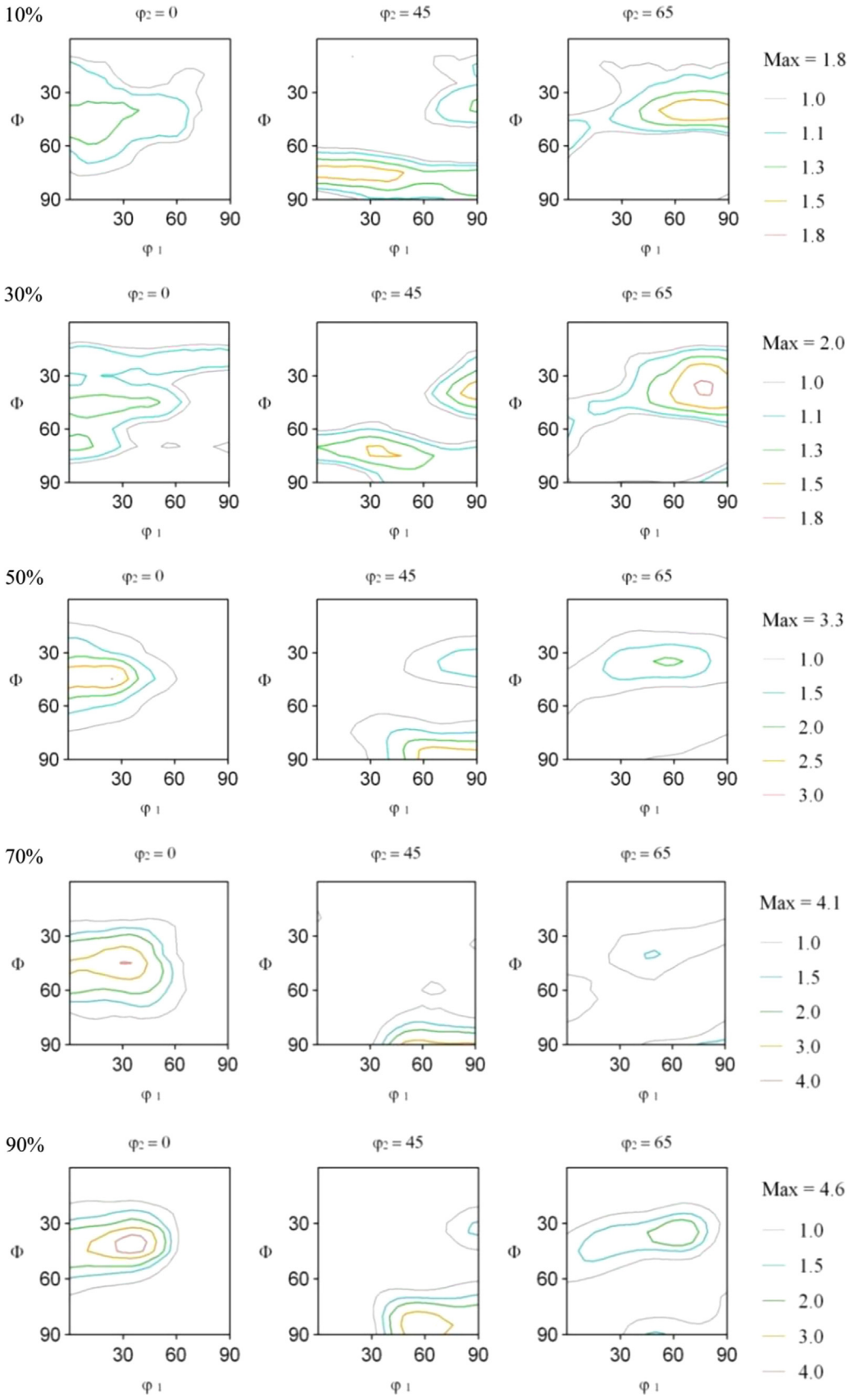

Fig. 5. ODF sections at φ_2=0°, 45° and 65° of the UDR samples.

3. Results and discussion

3.1. Deformation texture

Fig. 2 shows the macro and microtextures of the as-received Incoloy 800H/HT. For ease of comparison of the textures of all samples only the 3 important sections of ODF are illustrated and discussed here. We selected ODF sections at $\varphi_2=0^\circ$, 45° and 65° since they demonstrate the common FCC deformation and annealing texture features: α, β fibers and S component. Fig. 3 illustrates the major components and their positions where B, G, S, and Cu stand for brass, Goss, S and copper components respectively. Similarly B_T, G_T, S_T, and Cu_T show the ND rotated components. As Fig. 2 illustrates, both macro (XRD) and micro(EBSD) textures of Incoloy 800H/HT show a weak texture with no preferred orientations. Coarse grains and twinning have resulted from the hot rolling deformation history of the alloy.

Textures of the UDR and CR samples are depicted by pole figures (PF) and selected ODF sections. Fig. 4 shows the (111) PF for these samples at different rolling reductions. It is well-known that FCC materials develop two different types of rolling textures based on the materials structure (e.g. SFE, grain size, etc.) and the processing parameters (e.g. strain rate, strain path, rolling temperature, etc.) [18,21]. In general, low SFE materials tended to form the brass-type texture while high SFE materials favored the copper-type texture upon rolling. Similarly, it was found that low and high strain rates would encourage copper-type and brass-type textures, respectively [21].

Incoloy 800H/HT has low stacking fault energy (< 100 mJ/m^2) due to its alloying elements [32]. Therefore it is expected to have the FCC "alloyed" or brass-type texture rather than "pure metal" or copper-type [33]. Comparing the initial (111) PF (Fig. 2) with the rolled samples, one can observe the differences. More or less, all samples show typical brass-type texture, although there are some differences in the strength of maxima in UDR and CR, particularly at higher reductions (e.g. 90% UDR vs. 90% CR), which will be addressed later. We have extracted selected ODF sections to give a better illustration and more precise comparison between the samples, as previously mentioned. Figs. 5 and 9 show these ODF sections for the UDR and CR processed samples.

In order to characterize the deformation texture, we first focused on the UDR samples. As Fig. 5 illustrates, upon applying 10% deformation by UDR, we observed a weak texture with a combination of G, B, Cu and S components. This can be identified by $\varphi_2=0^\circ$, 45° and 65° ODF sections. After 30% reduction, the texture, represented by the same components, was strengthening. The $(221)\langle 2\bar{3}2\rangle$ component, which was very close to the S component is moving toward the brass component ($\varphi_2=45^\circ$ ODF section). Upon further reduction to 50%, we observed a strong texture consisting of B and G components. By increasing the rolling strain to 70%, Cu and G components gradually diminished while B component was strengthened. This trend continued to 90% reduction, where B component proposed itself as the dominant texture. Consequently, the final texture after 90% reduction was the typical brass type $(110)\langle 11\bar{2}\rangle$ rolling texture.

The transition of the near S component $(221)\langle 2\bar{3}2\rangle$ is clearly depicted in the β fiber (Fig. 6). By increasing the rolling strain, B component gradually intensified. Particularly, comparing the 50% and 70% processed samples one can observe the transition between near S components towards B component. In order to compare these components quantifiably, Fig. 7 shows the volume fraction of rolling texture components as a function of deformation strain. As discussed earlier, B and G components gradually increased in strength while Cu component decreased. The $(112)\langle 1\bar{1}1\rangle$ component increased up to 50% and then, upon the transition to B component, it reduced. This is in accordance with Wassermann's model that also has been reported elsewhere [19,30,34]. Due to the high multiplicity factor of S component, produced by slip at early deformation stages [35], we did not include its volume fraction in the figures. Fig. 5 depicts how S components are presented strongly in the $\varphi_2=65^\circ$ ODF section at 10% and 30% deformations. However by increasing the rolling

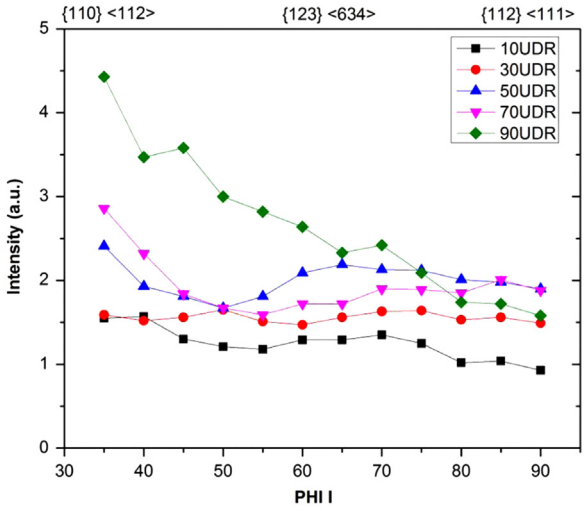

Fig. 6. β Fibers for the UDR samples.

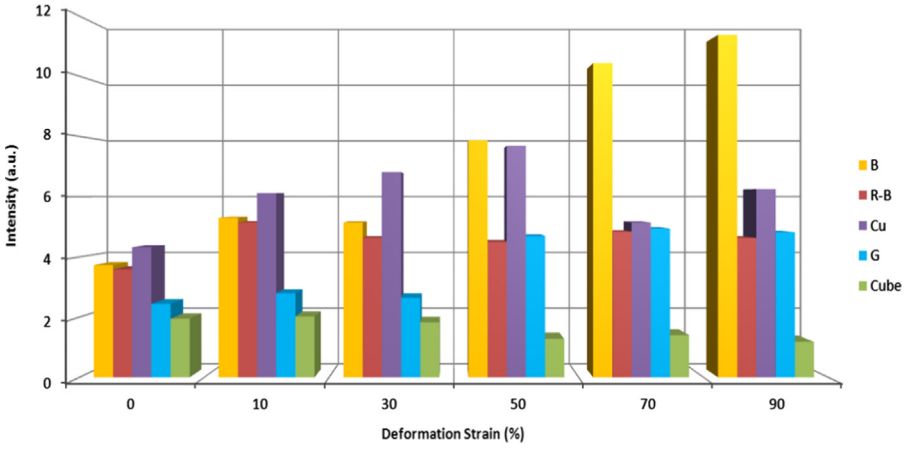

Fig. 7. Volume fractions of texture components in UDR samples at different deformation strains.

strain beyond 30%, S component was weakened. It is significant that the relatively low intensity in macrotexture is in agreement with the measurements of Saleh et al. [24] and Bracke et al. [28].

In their comprehensive review on brass-type texture, Leffers and Ray [21] state that deformation twinning is mainly responsible for the formation of brass-type texture. Other researchers also state that all materials showing brass-type texture exhibit extensive twinning [21,35]. In order to validate this for Incoloy 800H/HT, we analyzed the deformed samples by EBSD. Fig. 8 shows the orientation map of a 10% deformed sample. The most favorable orientation for twinning required to accommodate rolling strains is $(110)\langle 11\bar{2}\rangle$ [20]. As documented [21], at the earlier stages of deformation, twinning was typically restricted to a (111) plane. This fact can be clearly observed in Fig. 8 where twins were elongated in the grains with (111) and (112) planes (blue and purple colors). On the contrary, the annealing twins in other grains can be distinguished as they were generally singular, wider and elongated in all grain widths. Comparing this observation with Fig. 2, we see that some of the twins were present in the as-received structure. To elucidate the orientation relationship between the twins and the parent grains, we prepared two subsets from two different grains. The (111) pole figure of the first subset in the (111) blue grain shows a common pole between the twins and the parent grains. The primary twin in FCC structure exhibits a 60° rotation around the ⟨111⟩ crystal axis [22]. In order to consider a boundary as a coherent twin boundary not only should the rotation be correct but also a boundary should coincide with the twinning plane. This will result in having a common pole in (111) PF on the subsets consisting of twins and parent grains. Similarly, this rotation will result in 3 common poles in (110) PF. The second subset in (100) red grain had a slightly different twinning occurrence. As can be seen in the subset region and associated PFs, there was a third orientation between the twin and the parent grain (yellow color). It seems that here the Schmidt factor of the grain was not appropriate for twinning so slip occurred first, and then twinning took place. In addition, the number of twins in this region was not as large as the previous case. Again this could be related to the difference in orientation of the grains. Most of the deformation twins are seen in or near Cu oriented grains (blue and purple colors), which is in accordance with the fact that Cu-oriented grains are the most favorable grains to accommodate the strains with twinning [20,21].

Although some studies report the strong (111)//ND component in rolling texture of FCC alloys [20,21,23], here it is not the case. A very high degree of latent hardening is attributed to the presence and formation of this component [20,21]. Perhaps the reason for the absence of this component in Incoloy 800H/HT TMP is that the twinning deformation is not sufficiently dominant to impose the latent hardening. The absence of this component has also been reported in other materials (e.g. Ag) [20,21]. By comparing various alloys with different SFEs, Sekine and Wang [20] claim that the (111) component can only be present in very low SFE materials. In addition, they state that fine twin lamellae, which are responsible for (111) grains formation, are more predominant in very low SFE materials with fine grains. This is clearly not the case for Incoloy 800H/HT. However, TEM observation needs to be done for better clarifying this.

In contrast to the UDR samples, the CR samples show slightly different texture after the sequential rolling deformation. Fig. 9 depicts the ODF sections of CR samples at different rolling reductions. Compared to UDR after 10% reduction, the CR sample shows a strong brass texture. As the deformation increased, the dominant texture component oscillated between B and B_T. Comparing the $\varphi_2=45°$ sections for CR samples, we found that the strength of the texture components gradually moved from B to B_T. Bhattacharjee et al. suggest that the two stable texture components for the cross-rolling deformation would be $(110)\langle 1\bar{1}2\rangle$ (B) and $(110)\langle 1\bar{1}1\rangle$ (ND rotated B) [12]. Upon unidirectional rolling, the grains will move to B component [12,36]. By further rotating the strain path around ND by 90° in a cross-rolling condition, the

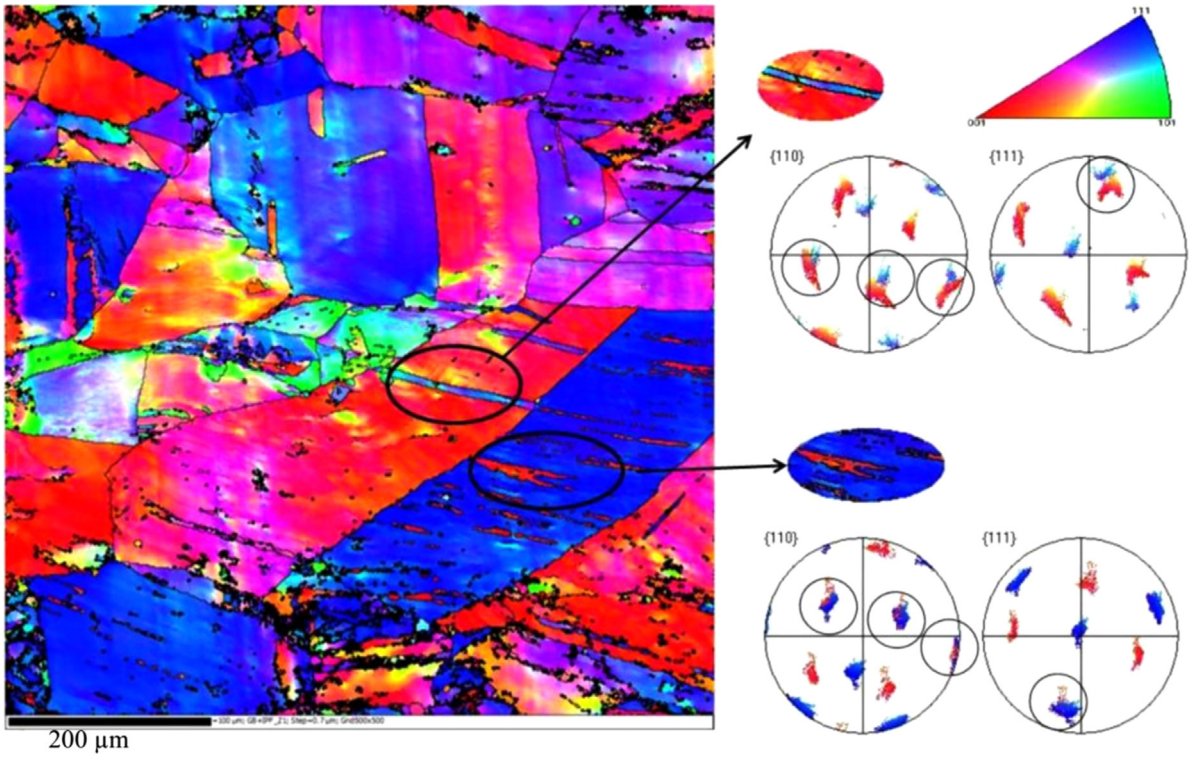

Fig. 8. Orientation map of 10% deformed sample showing extensive twinning in (111) grains. (For interpretation of the references to color in this figure, the reader is referred to the web version of this article.)

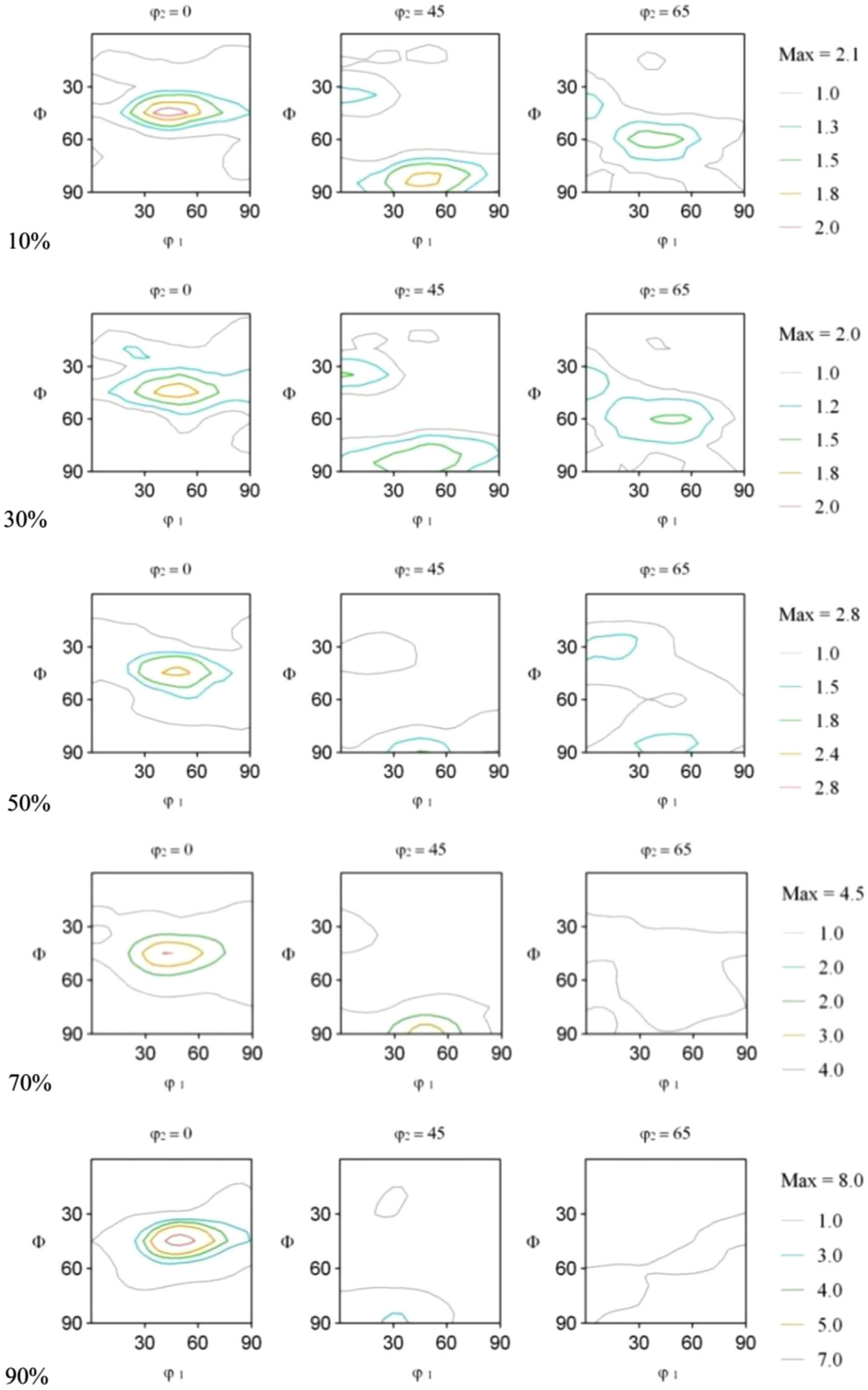

Fig. 9. ODF sections at φ_2=0°, 45° and 65° of the CR samples.

rotated B component will be driven. Therefore, the dominant texture of the cross-rolled samples would oscillate between B and ND rotated B.

Fig. 10 shows β fiber evolution in CR samples. Comparing this figure with Fig. 6, we observe that β fiber is unstable at CR condition. This result is in agreement with studies by Bhattacharjee et al. [12]

and Huh et al.[13], where they observed the same textural differences in CR and UDR samples.

In order to clearly demonstrate texture component changes in CR condition, Fig. 11 illustrates the volume fraction of rolling texture components as a function of deformation strain. As discussed earlier, B and B_T components gradually increased in strength while Cu and cube components decreased. G and S components remained almost unchanged. Therefore the deformation texture of Incoloy 800H/HT under the current CR condition at high deformation strains was a combination of B and B_T. After 90% deformation, B_T was the dominant texture. It is noteworthy that, depending on the last rolling path sequence, the final deformation texture of the CR samples at higher reductions is either B_T and Cu_T or normal B and Cu.

3.2. Annealing texture

We measured the textures of both UDR and CR samples after the recrystallization annealing and used a similar strategy to compare the textures. Fig. 12 illustrates the (111) pole figure of the annealed UDR and CR samples (UDRA and CRA). Compared to the deformed samples, the overall intensity of the pole figures was reduced. The PFs of UDRA and CRA samples show no significant differences up to 50% reductions. However in higher deformation regimes (i.e. 70% and 90%), we found sharp changes. These changes are clearer in ODF sections, which are shown in Figs. 13 and 14. In the annealed samples that were rolled up to 50% before annealing, $(013)\langle 0\bar{3}1\rangle$ and $(212)\langle 0\bar{3}1\rangle$ were the main components, although they are weak. The former and latter components were close to cube and S components, respectively. At low deformation stages, cube texture can be observed. This is in agreement with Sztwiertnia [26] who reports the minor cube component in a recrystallized Ag with low SFE. As noted from the PFs comparison, the main changes in annealing texture of the samples occurred at high deformations (i.e. 70% and 90%). The texture of the 70% UDR annealed sample was similar to the 50% UDR while the maxima were concentrated around G and $(001)\langle 1\bar{1}0\rangle$. By increasing the rolling strain to 90%, the texture was mainly B, G, and Cu with minor $(001)\langle 1\bar{1}0\rangle$ and S components. In contrast, annealed CR samples at 70% and 90% reductions depicted strong B with minor Cu and S components texture. This strong texture is also reported by Zhang and Sekine [37] in annealed pure silver that was cold rolled to 95% and also by Chowdhury et al. [34] in the recrystallization texture of cold rolled 304 austenitic steel. As stated by Chowdhury et al., if the deformation texture was close to brass, due to second order twinning, the recrystallization texture was likely to be close to copper component. It is evident that, depending on the rolling texture of the CR samples, the annealing texture at higher reductions is either B_T and Cu_T or normal B and Cu.

Most of the minor components that were observed in the recrystallized samples, such as $(326)\langle 83\bar{5}\rangle$ ($\{236\}\langle 385\rangle$ known as Recrystallized Brass: R-B), $(013)\langle 0\bar{3}1\rangle$ and $(114)\langle \bar{1}2\bar{1}\rangle$, could be driven from certain rotations (e.g. 40° $\langle 111\rangle$ twin rotations) of the deformed texture components. A detailed discussion on this can be found elsewhere [16,29]. The small differences between the positions of the assigned texture components could mainly be raised from various alloying elements in different studies, as declared by Schmidt and Lucke [29].

To elucidate the texture components differences in annealed UDR and CR samples, we acquired EBSD maps. Fig. 15 shows the differences between B and Cu components in the annealed 90% CR and 90% UDR samples. These images were taken to include about 2000 grains to obtain reasonable grain statistics. As illustrated in Figs. 13 and 14, the texture of 90% UDRA samples is a combination of G, Cu and R-B, while 90% CRA samples exhibit a strong brass texture. The results from macrotexture measurements could be validated by microtexture (EBSD) measurement. Fig. 15 illustrates the EBSD orientation maps for 90% UDRA and 90% CRA samples highlighting two major components: B and Cu. As shown, the 90% CRA sample has a high number of B-oriented grains (~25%) while 90% UDRA has fewer (~15%). However, 90% UDRA exhibits about 23% Cu-oriented grains in contrast with

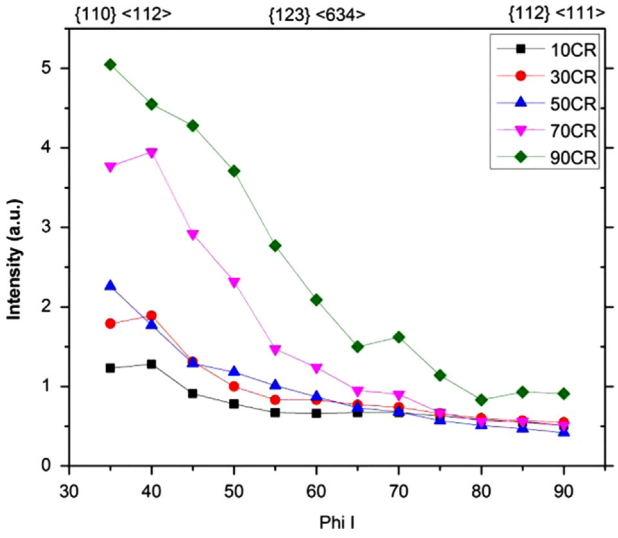

Fig. 10. β Fibers for the CR samples.

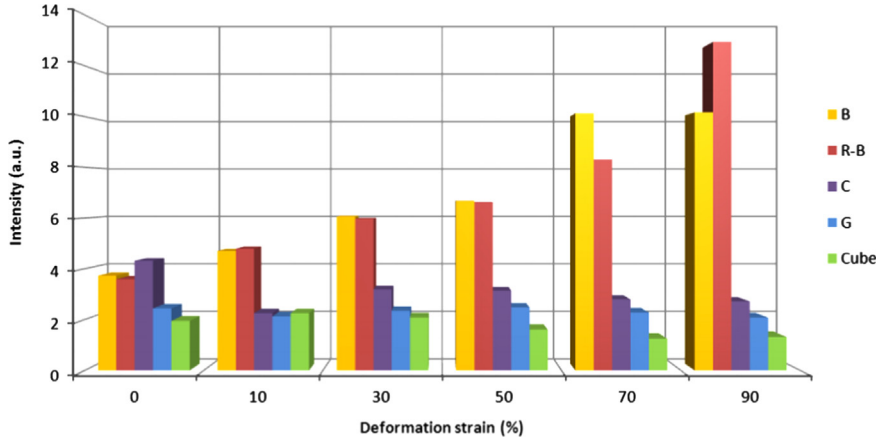

Fig. 11. Volume fractions of texture components in CR samples at different deformation strains.

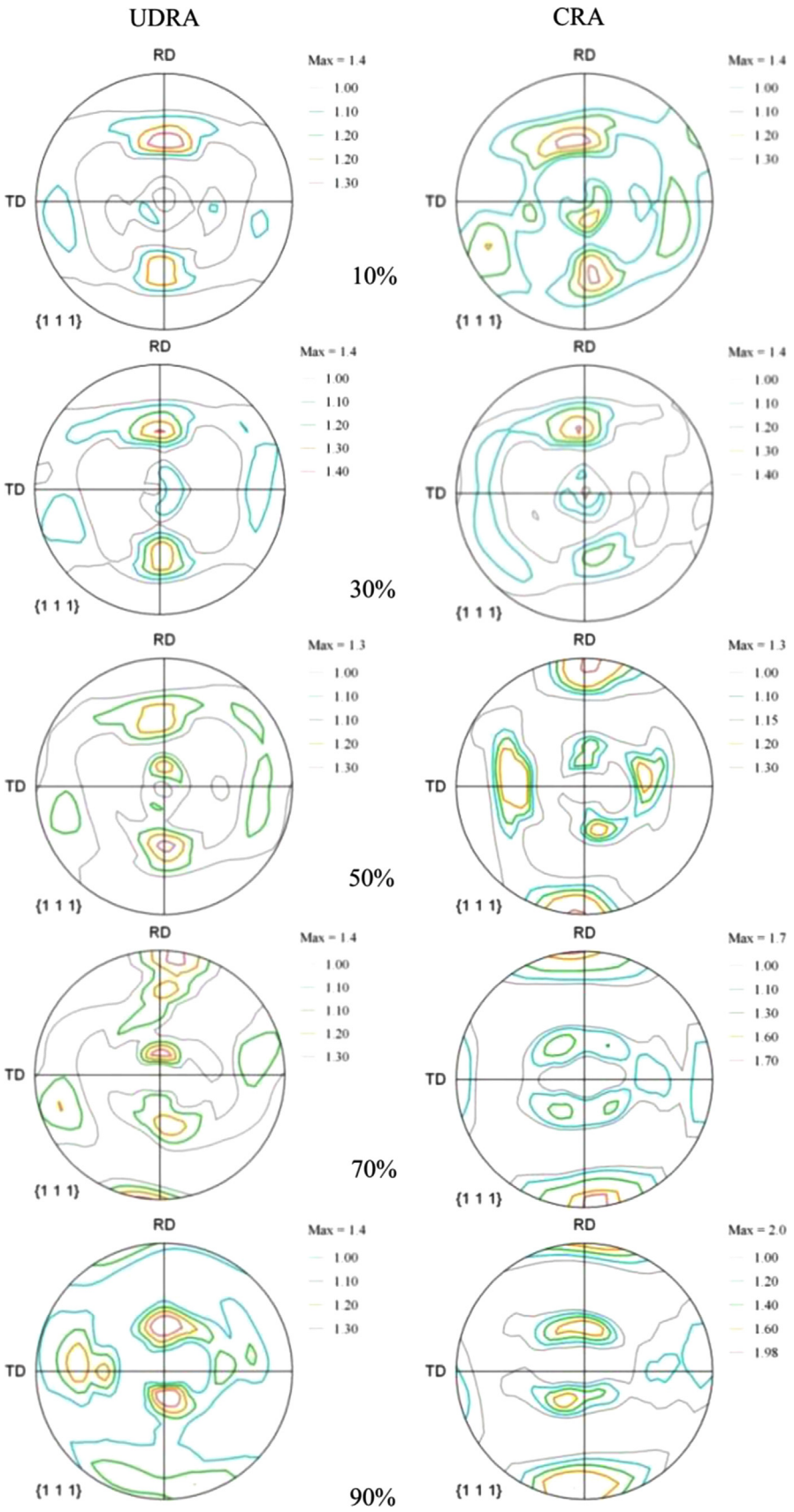

Fig. 12. (111) PFs of the CR and UDR samples.

only ~9% in 90% CRA. R-B and G components show similar trends to Cu. The R-B and G oriented grains fractions were about 16% and 12% for UDRA whereas the contribution of these components was reduced to 8% and 6% for the 90% CRA sample. Therefore, as a result, two different annealing textures have formed upon rolling after different strain paths.

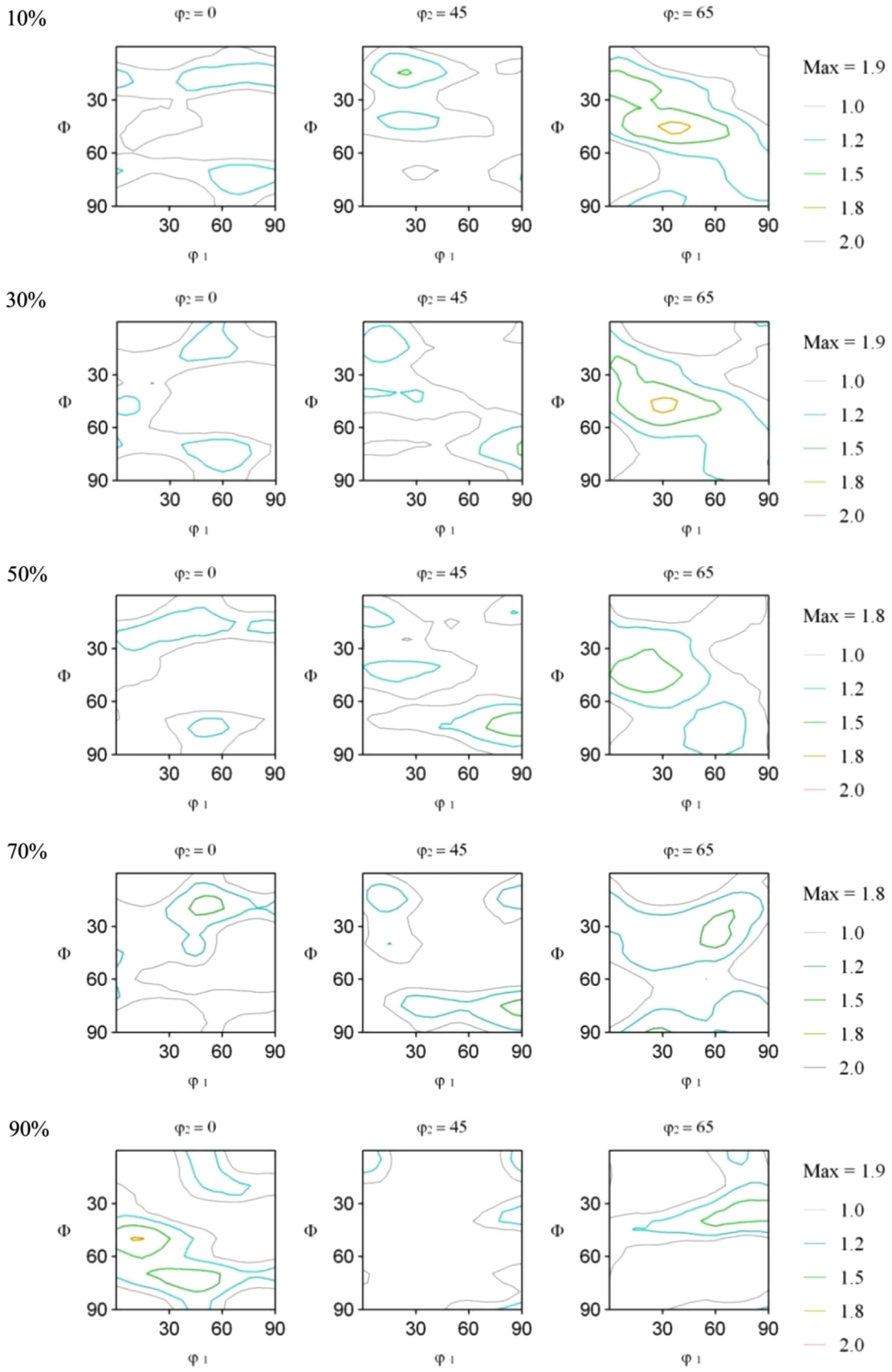

Fig. 13. ODF sections at φ_2=0°, 45° and 65° of the UDRA samples.

The retention of B component in recrystallization texture is reported in other studies on austenitic steels [24,28]. This texture retention could be attributed to nuclei growing inside the deformation grains, which would result in some B-oriented grains upon annealing [24]. Moreover, it is suggested that homogeneous distribution of deformation in the structure would make no preferable

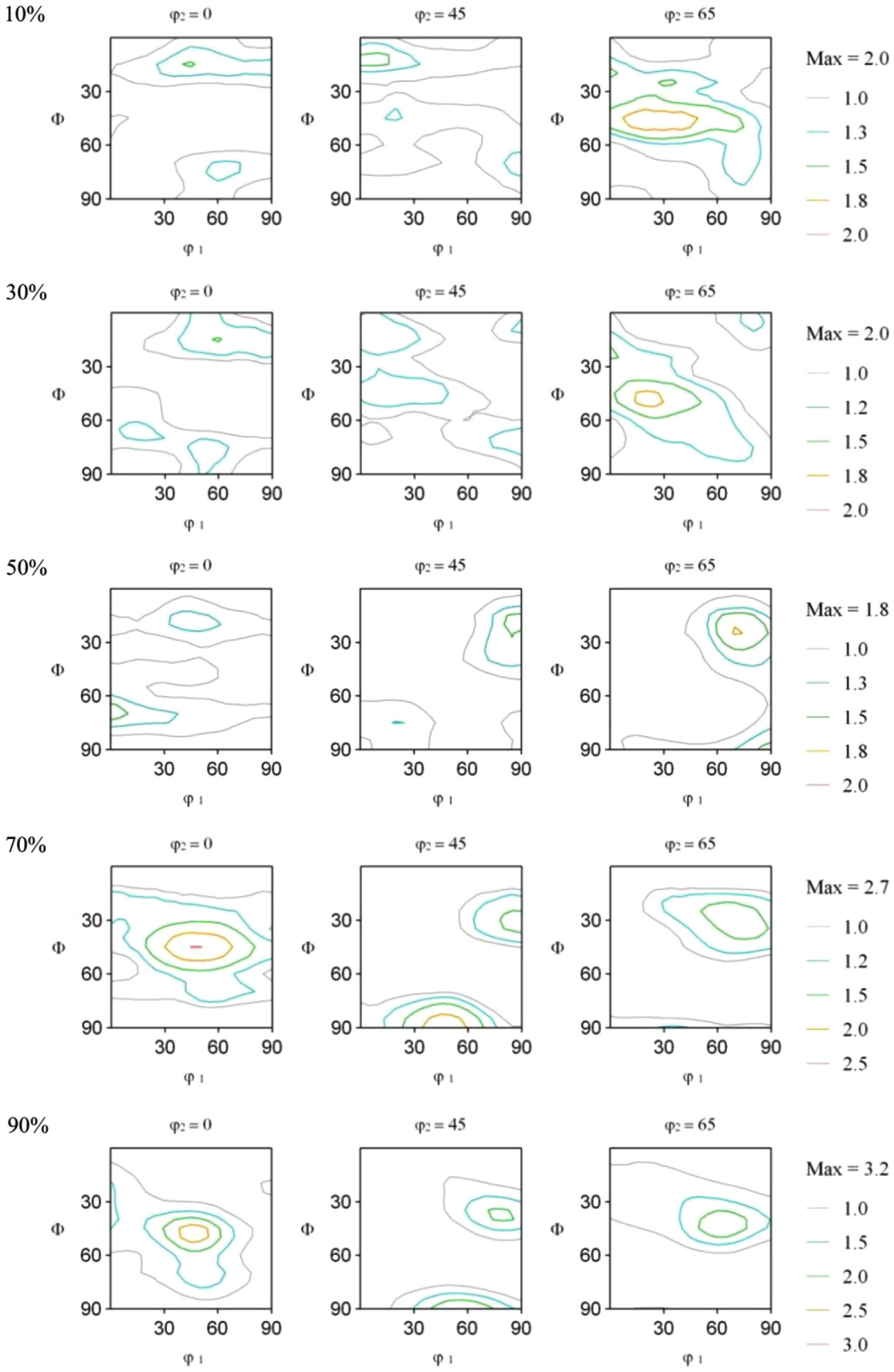

Fig. 14. ODF sections at φ_2=0°, 45° and 65° of the CRA samples.

orientation for nucleation. Therefore with random nucleation, rolling texture can be retained [28]. This behavior is only observed for Incoloy 800H/HT CR samples and it could be related to the cross-rolling process and its effect on the nucleation and growth. The mechanism of grain nucleation and growth in annealing CR and UDR samples is uncertain and is currently under investigation by the authors.

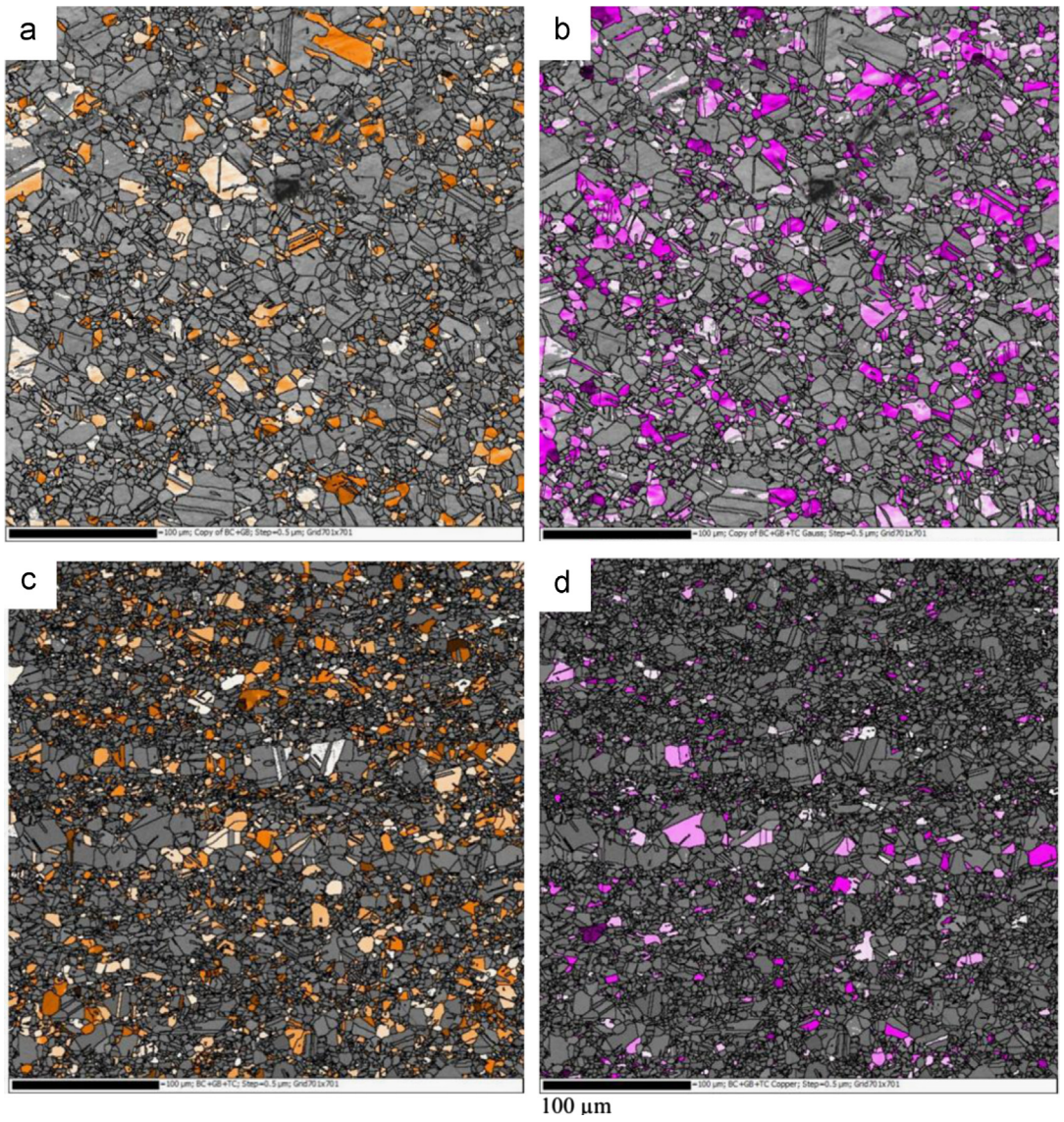

Fig. 15. Grain orientation maps of (a and b) 90% UDRA and (c and d) 90% CRA samples showing (a and c) brass-oriented grains and (b and d) copper-oriented grains (TD plane).

The manufacture of Incoloy 800H/HT with different textures would be of great interest to those who design and fabricate with this material. Texture can influence a wide range of material properties including formability, weldability, creep, oxidation and radiation damage [14,18,22]. We are currently investigating the oxidation resistance of the processed samples in super-critical water and preliminary results indicate that texture optimizing can improve alloy's oxidation resistance.

4. Conclusion

We carried out a comprehensive textural study of the deformed, through various rolling strains with two different rolling modes, and annealed samples of Incoloy 800H/HT. We draw the following conclusions based on our present results:

1. The final deformation texture for UDR samples, upon rolling to 90% reduction, was a typical brass texture while the dominant texture of the cross-rolled samples oscillated between B and ND rotated B.
2. Deformation twinning influenced the texture from the early stages of deformation. Microtexture analysis showed the important mechanisms of twinning and slip. The twinning can be traced at different stages of the transformation of texture.
3. The final recrystallized texture depends on the deformation mode applied before annealing; for UDR samples, a combination of G, Cu and R-B textures was dominant, while the recrystallization texture of CR samples after 90% rolling, retained the brass texture. In addition to the texture differences, CR samples have smaller grain size. Randomization of nucleation sites upon cross-rolling is one possible reason.
4. The retained B deformation texture in the annealing texture of CR samples at higher rolling reductions is related to a more homogeneous distribution of nucleation sites upon cross-rolling. Detailed studies are performing to elucidate the role of strain path on the nucleation and growth mechanism.

Acknowledgments

The authors express their gratitude to Cameco Corporation for their encouragement and support in the present investigation. The authors also would like to acknowledge the Cameco CRD-NSERC

program. Valuable discussions with Ali Sonboli and Mostafa Eskandari are greatly appreciated.

References

[1] U.S. DOE Nuclear Energy Research Advisory Committee and the Generation IV International Forum, A Technology Roadmap for Generation IV Nuclear Energy Systems, 2002.
[2] The OECD Nuclear Energy Agency for the Gen IV International Forum, Technology Roadmap Update for Generation IV Nuclear Energy Systems, 2014.
[3] W. Ren, R. Swindeman, Proceedings of the ASME 2010 Pressure Vessels and Piping Division, Bellevue, Washington, 2010.
[4] K. Mo, G. Lovicu, H.-M. Tung, X. Chen, Y. Miao, J.B. Hansen, J.F. Stubbins, J. Nucl. Mater. 443 (2013) 366.
[5] H.M. Tawancy, A. Ul-Hamid, A.I. Mohammed, N.M. Abbas, Mater. Des. 28 (2007) 686.
[6] L. Tan, L. Rakotojaona, T.R. Allen, R.K. Nanstad, J.T. Busby, Mater. Sci. Eng. A 528 (2011) 2755.
[7] Special Metals Corporation, The Story of the "INCOLOY Alloy Series" from 800 through 800H, 800HT, 2004.
[8] L. Tan, T.R. Allen, J.T. Busby, J. Nucl. Mater. 441 (2013) 661.
[9] G. Gupta, P. Ampornrat, X. Ren, K. Sridharan, T.R. Allen, G.S. Was, J. Nucl. Mater. 361 (2007) 160.
[10] L. Tan, K. Sridharan, T.R. Allen, J. Nucl. Mater. 348 (2006) 263.
[11] N.P. Gurao, S. Sethuraman, S. Suwas, Mater. Sci. Eng. A 528 (2011) 7739.
[12] P.P. Bhattacharjee, M. Joshi, V.P. Chaudhary, J.R. Gatti, M. Zaid, Metall. Mater. Trans. A 44 (2013) 2707.
[13] M.Y. Huh, S.Y. Cho, O. Engler, Mater. Sci. Eng. A 315 (2001) 35.
[14] O. Engler, V. Randle, Introduction to Texture Analysis, 2nd ed., CRC Press, Boca Raton, Florida, USA, 2010.
[15] B. Ravi Kumar, B. Mahato, N.R. Bandyopadhyay, D.K. Bhattacharya, Mater. Sci. Eng. A 394 (2005) 296.
[16] R.D. Doherty, D.A. Hughes, F.J. Humphreys, J.J. Jonas, D.J. Jensen, M.E. Kassner, W.E. King, T.R. McNelley, H.J. McQueen, A.D. Rollett, Mater. Sci. Eng. A 238 (1997) 219.
[17] F.J. Humphreys, J. Mater. Sci. 6 (2001) 3833.
[18] B. Verlinden, J. Driver, I. Samajdar, R.D. Doherty, Thermo-Mechanical Processing of Metallic of Metallic Materials, Elsevier, Pergamon Press, Oxford, UK, 2007.
[19] G. Wassermann, J. Grewen, Texturen Metallischer Werkstoffe, Springer, Berlin, 1962.
[20] K. Sekine, J. Wang, Mater. Trans. 40 (1999) 1.
[21] T. Leffers, R.K. Ray, Prog. Mater. Sci. 54 (2009) 351.
[22] F.J. Humphreys, M. Hatherly, Recrystallization and Related Annealing Phenomena, Elsevier, Oxford, UK, 2004.
[23] T. Leffers, Textures Microstruct. 22 (1993) 53.
[24] A.A. Saleh, E.V. Pereloma, A.A. Gazder, Mater. Sci. Eng. A 528 (2011) 4537.
[25] N. Rajmohan, J. Szpunar, Acta Mater. 48 (2000) 3327.
[26] K. Sztwiertnia, Mater. Lett. 123 (2014) 41.
[27] K. Sztwiertnia, Int. J. Mater. Res. 99 (2008) 178.
[28] L. Bracke, K. Verbeken, L. Kestens, J. Penning, Acta Mater. 57 (2009) 1512.
[29] U. Schmidt, K. Lucke, Texture Cryst. Solids 3 (1979) 85.
[30] S.G. Chowdhury, S. Das, P.K. De, Acta Mater. 53 (2005) 3951.
[31] K. Lucke, in: C.M. Brakman, E.J. Mittemeijer (Eds.), ICOTOM 7, Netherlands Society for Materials Science, Noordwijkerhout, Netherlands, 1984, p. 195.
[32] R.E. Schramm, R.P. Reed, Metall. Mater. Trans. A 6A (1975) 1345.
[33] I. Dillamore, W. Roberts, Acta Metall. 12 (1964) 281.
[34] S.G. Chowdhury, S. Datta, B.R. Kumar, P.K. De, R.N. Ghosh, Mater. Sci. Eng. A 443 (2007) 114.
[35] M. Sekine, N. Sakaguchi, M. Endo, H. Kinoshita, S. Watanabe, H. Kokawa, S. Yamashita, Y. Yano, M. Kawai, J. Nucl. Mater. 414 (2011) 232.
[36] S. Wronski, M. Wrobel, A.Baczmanski, K. Wierzbanowski, Mater. Charact. 77 (2013) 116.
[37] Z.R. Zhang, K. Sekine, Mater. Sci. Eng. A 423 (2006) 243.